Seasonal variations in the dynamic and thermodynamic response of precipitation extremes in the Indian subcontinent

Aditya Sengupta[1], Naresh Krishna Vissa[1*] and Indrani Roy[2]

[1*]Department of Earth and Atmospheric Sciences, National Institute of Technology Rourkela, Sundargarh, 769008, Odisha, India.
[2]University College London, Gower Street, London, WC1E6BT, UK.

*Corresponding author(s). E-mail(s): vissan@nitrkl.ac.in; vissanaresh@gmail.com;

Abstract

Precipitation extremes are a major impact-relevant implication of climate change. Rising temperatures increase the moisture holding capacity at a rate of $\approx \boldsymbol{7\% K^{-1}}$, called the Clausius-Claypeyron (CC) scaling, which can lead to intense precipitation which last for short duration. At a regional level, the scaling of extremes deviates from this expected scaling rate. Large scale circulation dynamics and local variability in thermodynamic influences are suspected to cause these deviation, but these drivers differ across seasons. In the present study, we use ERA5 reanalysis to evaluate the seasonal changes in precipitation-temperature scaling rates over the Indian subcontinent. We further determine the deviations from the expected CC scaling rate, and the precipitation extremes are decomposed to their dynamic and thermodynamic contribution across different seasons. It is found that significant seasonal contrast exists in the dynamic and thermodynamic contributions, with the latter dominating during the Indian summer monsoon season, while the former being higher during the pre-monsoon and post-monsoon season. Further analysis highlights that the lower dynamic contribution is attributed to drop in dew point temperatures and Convective Available Potential Energy during extremes. The primary drivers causing the extremes in different seasons are also pointed out, further improving the understanding of how the intensity and frequency of precipitation extremes changes spatially across different seasons, and what are the physical drivers causing these changes.

Keywords: Precipitation extremes, CC scaling, Dynamic and Thermodynamic processes, ERA5

1 Introduction

One of the most impact-relevant implications of climate change is extreme precipitation and its associated impacts (Fadhel et al, 2018). In recent decades, the intensity and frequency of precipitation extremes has increased (Alexander, 2016; Fischer and Knutti, 2016; Groisman et al, 2005; Guerreiro et al, 2018; Myhre et al, 2019; Papalexiou and Montanari, 2019; Pattanaik and Rajeevan, 2010; Westra et al, 2013) and are likely to increase further, under a warming climate (Ali and Mishra, 2018b; Fowler et al, 2021; Kharin et al, 2013; Mukherjee et al, 2018; Pfahl et al, 2017). These variations in the nature of short duration rainfall extremes at the daily and sub-daily timescales leads to rapidly developing flash floods as well as landslides, and debris flow that can cause severe damage to societies all over the world through adverse socio-economic impacts (Ali et al, 2021b; Fadhel et al, 2018; Fowler et al, 2021; Lenderink and van Meijgaard, 2008). Projecting changes in future extreme precipitation is a more complicated endeavor, as compared to the projections of future changes in near surface air temperature. Therefore, a method is required to project precipitation using its dependency on other climate variables, and temperature itself is one of the major climate variables that shows a strong relationship with average and especially extreme precipitation events (Herath et al, 2018). This relationship, also referred to as scaling (precipitation extremes as a response to changes in temperature) has a physical basis in the Clausius-Claypeyron (CC) relationship, according to which, low-level moisture rises at a rate of $\approx 7\% K^{-1}$, assuming no change in relative humidity and provided that the effect of large scale atmospheric circulation processes are negligible (Ali et al, 2018; Chen et al, 2022; Fowler et al, 2021; Lenderink and van Meijgaard, 2008; O'Gorman and Schneider, 2009; Trenberth et al, 2003; Zhang et al, 2019). This purely thermodynamic response of near-surface moisture to changes in surface temperature is what fuels comparable rises in extreme precipitation events, primarily driven by moisture convergence (Allan and Soden, 2008). Since, short-duration extremes are generally limited by availability of moisture in the atmosphere, the CC relation forms a reliable physical basis for the understanding of the response of precipitation extremes in a warming climate. Hence, to a first approximation, rainfall extremes are expected to scale at the same rate as that suggested by the CC relation (Fowler et al, 2021; Lenderink and van Meijgaard, 2008; Trenberth et al, 2003). This relationship has been used as a benchmark for interpreting changes to precipitation extremes (Ali et al, 2018; Ali and Mishra, 2017; Fischer and Knutti, 2016; O'Gorman, 2015). GCMs and coupled ocean-atmospheric models also predict a globally averaged scaling of $\approx 7\% K^{-1}$ for precipitation extremes.

The CC scaling relationship is quite robust, especially on a global scale (Fischer and Knutti, 2016; Guerreiro et al, 2018; Nayak, 2018; Westra et al, 2014), but in recent studies, both model simulations and observational studies have shown large deviations from the CC scaling (Ali and Mishra, 2017; Hardwick Jones et al, 2010; Park and Min, 2017; Pfahl et al, 2017; Vittal et al, 2016; Zhang et al, 2019) at a regional scale. This relation between short duration extreme precipitation intensities and short-term variability in temperature, at a local/regional scale, is what is termed as apparent scaling (Ali et al, 2018, 2021a; Bao et al, 2017; Fowler et al, 2021). This deviation of the apparent scaling from the value of $\approx 7\%K^{-1}$ (expected from the CC relation) arises as super-CC scaling (scaling $> 7\%K^{-1}$), mostly for sub-daily (mostly hourly) precipitation intensities (Ali and Mishra, 2017; Fowler et al, 2021; Hardwick Jones et al, 2010; Lenderink and van Meijgaard, 2008; Lenderink et al, 2017; Park and Min, 2017; Wang et al, 2017; Westra et al, 2014). It can also arise as sub-CC or even negative scaling observed primarily in the subtropics and tropics (Ali et al, 2018; Fowler et al, 2021; Hardwick Jones et al, 2010; Utsumi et al, 2011; Vittal et al, 2016; Zhang et al, 2017), indicating a decrease in precipitation intensity with increase in surface air temperature (SAT). These deviations are attributed to several confounding factors. Some of these factors include local cooling effects (Ali and Mishra, 2017; Bao et al, 2017) and moisture limitations at higher temperatures (Barbero et al, 2018; Lenderink et al, 2018). Another major source of deviations in scaling rates has been temperature seasonality (Ali et al, 2018; Zhang et al, 2017).

Apart from these, a major factor influencing the deviation from the expected CC scaling rate is the localized effect of large-scale circulation patterns, causing enhancement of local moisture availability through upward motions and moisture convergence (Dairaku and Emori, 2006; Emori and Brown, 2005; Moustakis et al, 2020; O'Gorman, 2015; O'Gorman and Schneider, 2009; Vittal et al, 2016). This dynamical influence also occurs through the transport of low level moisture from neighboring regions (Kumari et al, 2021). Thus, the large scale dynamics can play a significant role in deviating the scaling rates (Ali and Mishra, 2018a; Guerreiro et al, 2018; Lenderink et al, 2017; Liang and Zhang, 2021; Liu et al, 2020; Magan et al, 2020; Oueslati et al, 2019; Pfahl et al, 2017; Sudharsan et al, 2020; Yamada et al, 2021). Despite the existence of an extensive amount of literature, the diversity of apparent scaling patterns still remains a field of discussion (Bao et al, 2017, 2018; Barbero et al, 2018; Lenderink et al, 2018). It is clear that just the determination of scaling pattern on a regional level is not enough, since the sensitivity of the observed super-CC and sub-CC scaling to climate scaling is still quite uncertain (Fowler et al, 2021; Sudharsan et al, 2020). One also needs to understand the cause of the deviations in the apparent scaling rates from the expected climate scaling at a regional level. Furthermore, it is also necessary to quantitatively understand the role that large scale circulation and dynamical influences play in causing the deviations of apparent scaling rates.

The discrepancy between CC scaling and observed trend has been the most prominent in the tropics (Ali et al, 2021b). Recent studies (Ali and Mishra, 2018a; Pfahl et al, 2017; Vittal et al, 2016) used a proxy method developed by O'Gorman and Schneider (2009) to evaluate the role of the dynamic and thermodynamic contribution to precipitation extremes (discussed further in section 3) and concluded that dynamic components dominate the contribution to extremes on a global scale. Over the Indian region, there have been a few studies that have attempted to decompose the precipitation to the dynamic and thermodynamic contributions, to assess the primary drivers responsible for the extremes. However these studies have either been confined to urban locations or only to certain sites with suitable data availability (Ali and Mishra, 2018a), or have only focused on particular extreme events (Sudharsan et al, 2020). Kumari et al (2021) were the first to comprehensively understand the dynamical and thermodynamic aspects of light and heavy precipitation events over India using ERA5 reanalysis, over an appreciably large time-span. While, all of these studies over India have concluded that dynamic contribution to precipitation extremes dominates the thermodynamic contribution over the annual period, a seasonal analysis of the same has never been attempted before.

It is essential to understand how the nature of the contributions of the dynamical and thermodynamic drivers to precipitation extremes changes seasonally, because rainfall extremes are on the rise in the Indian subcontinent and will continue to rise (Saha and Sateesh, 2022). Thus, in the present study, we discuss the nature of the physical causes affecting the deviations of apparent scaling rates from the expected climate scaling in the Indian subcontinent and how the dynamic and thermodynamic controls on the deviations vary seasonally. We first determine the apparent scaling rates for precipitation extreme events (exceeding P95 threshold) at a daily timescale, over the Indian subcontinent, using ERA5 precipitation and temperature data. The motivation behind using ERA5 is its spatial continuity and high spatial and temporal resolution. We determine the scaling response against both surface air temperature (SAT) and dew point temperature (DPT) as covariates, across different seasons (pre-monsoon, monsoon and post-monsoon), and then we use the proxy method developed by O'Gorman and Schneider (2009) to determine the contributions of dynamics and thermodynamics in causing the deviations in scaling. Following this, we try to determine the role of the large scale dynamics and thermodynamics during these extremes using a composite anomaly method to determine the climatological features associated with the said extremes, to validate the results of dynamic and thermodynamic contribution obtained using the proxy method. The motivation behind doing such an analysis is to provide an overview of precipitation extremes and associated dynamical features, in the warming period of the late 20^{th} and early 21^{st} century (1979-2020). An understanding of the seasonal changes in the dynamic and thermodynamic response is critical due to the different rain-bearing systems and precipitation mechanisms in the region across different seasons, which are discussed in detail in section 2 along with the details of the study area and data used. The methodology employed for determination of scaling rates, as well as for decomposing the precipitation to the constituent dynamic and thermodynamic contributions, and the methods utilized for the determination of climatological features are highlighted in section 3 . In section 4, the results of the study are presented and discussion on the inferences drawn from the results, with an attempt to emphasize the physical reasoning behind the deviations of apparent scaling, and the major conclusions from the analysis are summarized in section 5.

2 Study Area and Data

The Indian subcontinent region is prone to different precipitation mechanisms and rain-bearing systems across seasons (Anandh and Vissa, 2020), the most significant of which is the Indian summer monsoon (ISM) season which occurs during the summer months (JJAS), starting from June and lasting till September. The monsoon circulation causes heavy rainfall over Central and Southern India due to the northward shift of the Tropical Convergence Zone and formation of a synoptic scale heat low over northwestern India (Francis and Gadgil, 2006)(Krishnamurthy and Ajayamohan, 2010)(Romatschke et al, 2010). In the pre-monsoon (MAM or March, April and May), and post-monsoon (OND or October, November and December) seasons, tropical cyclonic storms with strong torrential winds and are a primary source of heavy precipitation (Evan and Camargo, 2011; Hamada et al, 2014; Mohanty et al, 2012; Tyagi et al, 2011; Vissa et al, 2013), while thunderstorms and mesoscale convective systems over land and ocean, also cause cloudbursts leading to debris flow and flash flooding (Dimri, 2013; Kikuchi and Wang, 2010; Romatschke et al, 2010; Virts and Houze, 2016). Hence, it is imperative to understand the seasonal changes in the dynamic and thermodynamic response of extremes over the Indian subcontinent (see Fig. 1) ranging, in the meridional direction, from 0^oN to 40^oN, and zonally from 60^oE to 100^oE.

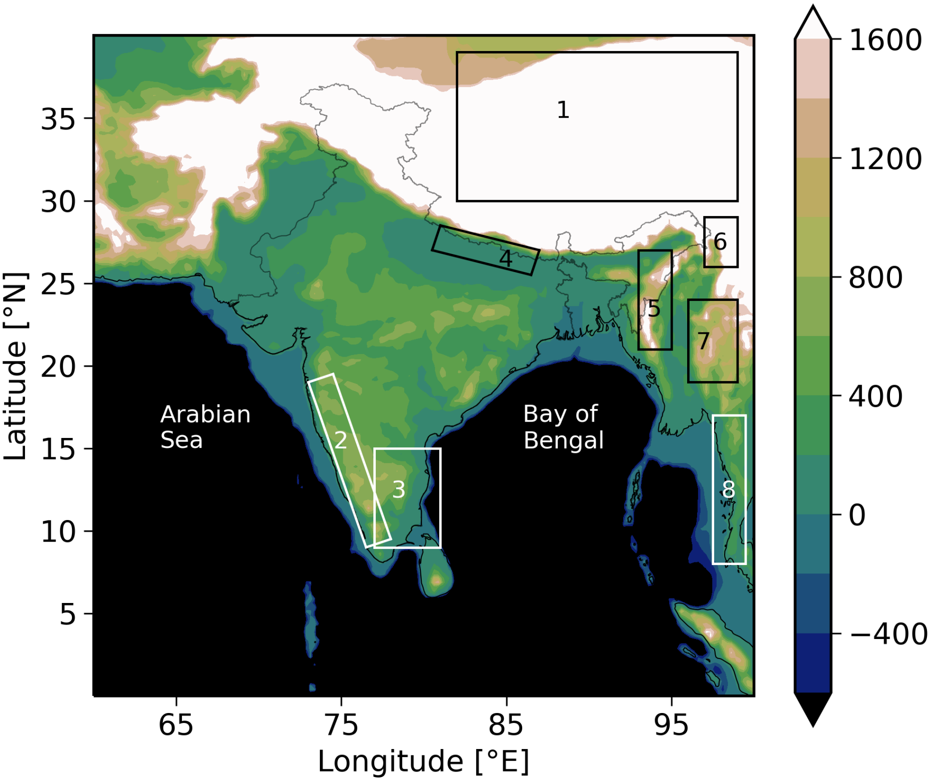

Fig. 1 Study area and the elevation relative to sea level (in the background) in the Indian subcontinent region. The numbered regions in the figure are as follows - **1.** Tibetan Plateau; **2.** Western Ghats **3.** South-East Peninsular India; **4.** Foothills of the Himalayas; **5.** Arakan Mountains; **6.** Hengduan Mountains; **7.** Shan Plateau; **8.** Tanasserim Hills.

We first determined the seasonal changes in the scaling rates, i.e. response of extremes to changes in temperature, over the study area using near surface temperature i.e. air temperature at 2 m (SAT) and dew point temperature (DPT) and total precipitation hourly data from the European Center for Medium Range Weather Forecasting (ECMWF) Re-Analysis 5th Generation (ERA5) dataset on single levels (Hersbach et al, 2020). The total precipitation hourly data was resampled to a daily timescale for determination of scaling of daily precipitation extremes. Hourly gridded data on a single level was obtained for the time-period of 1979-2020. The dataset was preferred over other reanalyses for its high spatial resolution ($0.25^o \times 0.25^o$) and temporal resolution. Some recent studies have compared the performance of ERA5 against other reanalysis products and have shown that ERA5 is highly reliable for hydrological applications including the study of extremes (Bhattacharyya et al, 2022; Mahto and Mishra, 2019; Ougahi and Mahmood, 2022).

Table 1 Data sets used for the analysis

Source	**Parameters**	**Spatial Resolution**	**Temporal Resolution**	**Pressure levels**
ERA5 single levels	i) Total precipitation	$0.25^o \times 0.25^o$	Hourly *	-
	ii) Temperature at 2m	$0.25^o \times 0.25^o$	Hourly *	-
	iii) Dew point temperature at 2m	$0.25^o \times 0.25^o$	Hourly *	-
	iv) Vertically Integrated Moisture Divergence	$0.25^o \times 0.25^o$	Hourly *	-
	v) Convective Available Potential Energy	$0.25^o \times 0.25^o$	Hourly *	-
ERA5 pressure levels	i) Zonal and Meridional Winds	$0.25^o \times 0.25^o$	Hourly *	850 hPa
	ii) Specific Humidity	$0.25^o \times 0.25^o$	Hourly *	1000 - 50 hPa
	iii) Vertical wind	$0.25^o \times 0.25^o$	Hourly *	1000 - 50 hPa

* All the data sets are obtained for the period of 1979-2020 and was resampled temporally to 24-H resolution for scaling of daily precipitation extremes.

For the determination of climatological features, as well as dynamic and thermodynamic mechanisms during the precipitation extremes, and for determination of dynamic and thermodynamic contribution to precipitation extremes, we used ERA5 hourly data on both single level and pressure levels. Parameters such as Vertically Integrated Moisture Convergence (VIMC), Convective Available Potential Energy (CAPE) were analyzed, and vertically integrated northward and eastward water vapor fluxes were used for the determination of Vertically Integrated Moisture Transport or VIMT. Furthermore, hourly data on pressure levels, such as zonal and meridional winds, specific humidity, temperature and vertical wind were primarily used for the determination of Low Level Moisture Transport (LLMT) and the decomposition of dynamic and thermodynamic contributors to precipitation extremes. A detailed description of the parameters used for this study are presented in Table 1.

3 Methodology

3.1 Determination of the seasonal changes in apparent scaling rates

The binning method has been employed for the determination of scaling rates, which has been shown to provide robust results in previous studies (Ali et al, 2021a; Ali and Mishra, 2017; Blenkinsop et al, 2015; Hardwick Jones et al, 2010; Herath et al, 2018; Hosseini-Moghari et al, 2022; Lenderink and van Meijgaard, 2008; Park and Min, 2017; Wasko et al, 2018). To employ the method, first, a threshold value of 1mm/day for daily precipitation intensity was chosen to restrict the analysis to only 'wet days' for each season (pre-monsoon; monsoon; and post-monsoon), at a particular grid point. Then the seasonal data for the wet days over the entire span of 42 years was chosen, and the corresponding temperature values i.e. SAT/DPT, at a daily timescale were extracted to start the binning process at that grid point. Following the work of Herath et al (2018), the precipitation data, at each grid point, was then divided and placed into 20 equal frequency temperature bins (of the corresponding grid point). The motivation behind using equal frequency binning over equal width binning was to ensure that all bins have the same amount of data values, thus preventing the highest and lowest temperature bins from having fewer pairs, as temperature is generally normally distributed. Moreover, using equal width bins causes empty bins to be ignored, leading to a distortion in the determined precipitation-temperature scaling relationship. This was done in an attempt to minimize any unnecessary effect of the employed methodology on the determination of apparent scaling rates.

After the binning, the 95th percentile of precipitation intensity, as well as mean temperature (SAT/DPT) in each bin was estimated, and a linear regression was fitted on the logarithm of P95 and mean SAT/DPT for each grid point following the work of Ali et al (2018, 2021a); Zhang et al (2019) -

$$\log P_i = \beta^0 + \beta^1 T \tag{1}$$

The slope (β^1) and p-value associated with the regression, were obtained to determine the scaling rates and significance of the fit. The apparent scaling rate (α) was then calculated using the relation (Ali et al, 2018, 2021a; Zhang et al, 2019),

$$\alpha = \frac{dP_i}{dT} = 100 \cdot (\exp(\beta^1) - 1) \tag{2}$$

where the term P_i represents the precipitation intensity and T represents one of the temperature covariates used for the present analysis i.e. either SAT or DPT. Recent studies (Ali and Mishra, 2017; Zhang et al, 2019; Fowler et al, 2021) pointed out that high SAT values generally correspond to drier conditions, leading to low moisture availability. In other words, at higher temperatures, although the moisture holding capacity of the atmosphere increases, the absolute humidity doesn't increase, so the relative humidity declines. This phenomenon is most prevalent in the tropics and leads to low magnitude or even negative scaling rates. DPT takes the reduction in Relative Humidity

(RH) with increasing temperatures into consideration, and thus the moisture changes in the atmosphere are included in the assessment of scaling. Essentially, as RH decreases with increasing temperatures, DPT declines more strongly as compared to SAT, and this leads to more robust results of apparent scaling , thus strengthening the fundamental understanding that changes in DPT (moisture availability) is the primary driver for precipitation extremes (Fowler et al, 2021). Thus, near surface DPT is a more appropriate choice for determination of scaling rates, especially over the tropics . Hence, for the present analysis, more emphasis was given to the scaling rates obtained against the DPT covariate.

3.2 Determination of dynamic and thermodynamic contribution to extreme precipitation events

The deviations of apparent scaling rates and super-CC scaling rates in the tropics was first justified by O'Gorman and Schneider (2009), with a large ensemble of climate models. They pointed out that the simulation of precipitation extremes in the tropics were not reliable, and they proceeded to address these inconstancies with a physical basis (O'Gorman and Schneider, 2009), where they highlighted the importance of large scale dynamics and showed that improvements in the simulation of upward velocities in a climate model can improve the predictions of precipitation extremes and provided a critical proxy for estimation of dynamic and thermodynamic contributions to precipitation extremes. We employed this proxy method to disentangle the contribution to precipitation extreme due to dynamic and thermodynamic factors. The method has also been used by Pfahl et al (2017) and Vittal et al (2016) to understand the relative importance of dynamic factors, such as changes in vertical winds in a warming climate, on the intensity of precipitation extremes and its scaling.

The method is based on the physical assumption that changes in precipitation extremes with climate depend on the changes in the moist-adiabatic temperature lapse rate, in the upward velocity, and in the temperature when the extremes occur. The scaling of precipitation is approached in terms of relating the intensity of precipitation extreme, P_e to the vertical velocity in pressure coordinates, i.e. ω_e, associated with the extreme event, and the vertical derivative of the saturation specific humidity with respect to pressure assuming a moist adiabatic lapse rate, such that,

$$P_e \approx -\left\{\omega_e \frac{dq_s}{dp}\Big|_{\theta^\star}\right\} \tag{3}$$

Here, $\{\cdot\}$ represents the mass weighted integral of the product of the upward vertical velocity (ω_e) and vertical derivative of q_s at constant saturation equivalent potential temperature ($\theta^\star$) over the troposphere as described in the works of Pfahl et al (2017) and Ali and Mishra (2018a). The equation is converted to equality by multiplying a constant called precipitation efficiency factor on the right-hand side, which is taken as 1 for this study following the work of Ali and Mishra (2018a). In the present study, the P_e value is considered as the estimate of all precipitation events exceeding the 95th percentile of precipitation on all wet days. The estimate is calculated by first determining the extremes exceeding the threshold of 95th percentile, and the corresponding vertical profiles of specific humidity, and vertical velocity at pressure levels ranging from surface ($1000hPa$) to the pressure level below $\approx 50hPa$ following the work of Pfahl et al (2017) and Ali and Mishra (2018a). Instead of determining the saturation specific humidity at each pressure level, the specific humidity has been used instead to take into consideration the vertical variations in specific humidity and thus changes in moisture during extreme events. It is an appropriate approximation, since the vertical profiles of q and q_s are expected to be similar to each other during precipitation extremes, since saturation has already occurred (see supplementary Fig. S1). In addition, the variations in near surface humidity should be taken into consideration for better determination of precipitation estimates for extremes with relatively low intensity.

After this, the parameters obtained (i.e. vertical profiles of vertical velocity and saturation vapour pressure), are used as input in the scaling relationship to obtain the overall scaling as the precipitation estimate. It is important to note that the scaling relationship gives the estimates in mm/s which are then further multiplied by the precipitation duration to get the estimates. Here, the thermodynamic contribution is determined with a constant value of (ω_e) (mean of all values corresponding to extreme events). In other words, to calculate the thermodynamic contribution, the variation in the upward vertical velocity (ω_e) corresponding to extreme precipitation was neglected, but was used to determine the estimate. The dynamic contribution is estimated by subtracting the thermodynamic contribution from the precipitation estimate (Ali and Mishra, 2018a; O'Gorman and Schneider, 2009; O'Gorman and Schneider, 2009; Pfahl et al, 2017; Williams and O'Gorman, 2022)

$$P_e = Dyn\ +\ Thermo \tag{4}$$

3.3 Determination of dynamic and thermodynamic mechanisms during extreme precipitation

In the present study, a composite analysis of CAPE, VIMC, LLMT and VIMT during extreme precipitation events was carried out to determine the thermodynamic and dynamical processes associated with precipitation extremes using the ERA5 precipitation data and meteorological data on single levels and pressure levels. Here, CAPE represents the instability (thermodynamic index) required for precipitation to occur. Positive CAPE represents conditions suitable for air parcels to rise, whereas negative CAPE causes air parcels to sink. VIMC, VIMT and LLMT represent dynamical processes. LLMT and VIMC give an indication of both the available low level moisture at a region, and moisture divergence gives an indication of the transport of moisture from or to a region. The negative/positive value of divergence signifies the transport from/to a region, which is referred to as divergence and convergence of moisture (Kumari et al, 2021). CAPE is the vertically integrated buoyancy of adiabatically lifted sub-cloud air and has been used in previous studies as a thermodynamic index for precipitation extremes. Since, convective potential is a major factor influencing precipitation intensity, it is an important measure for determining the role of thermodynamic changes during extreme events. The hydrological cycle and its changes in a warming climate are a major governing factor for precipitation extremes, and moisture transport is an important component of the hydrological cycle, and a warming climate is projected to have a direct impact on increasing low level moisture availability. Hence, LLMT is a major dynamical index to study the low level local moisture availability of the region. LLMT is calculated using the specific humidity (q), zonal (u) and meridional (v) winds at 850 hPa (Lélé et al, 2015; Kumari et al, 2021).

$$LLMT = q_{850} \cdot U(u, v)_{850} \tag{5}$$

Further, VIMT is used as an additional dynamical index, which is essentially the vertical summation of the product of specific humidity and zonal and meridional winds at different atmospheric levels. In the present study, VIMT was estimated using ERA5 vertically integrated eastward and northward moisture flux. The equation for VIMT is given below that has been used in earlier studies (Kumari et al, 2021; Mishra et al, 2012; Yang and Dominguez, 2019; Roxy et al, 2017),

$$VIMT = \frac{1}{g}\int_{sur}^{ToA} q \cdot U(u,v)dP \tag{6}$$

Where, q is the specific humidity, U represents the zonal and meridional winds, integrated over the entire atmospheric column, and g is the acceleration due to gravity. Moisture Convergence, or VIMC, has been chosen as a dynamical index in addition to LLMT and VIMT, to analyze the moisture content available over the region from the surface to the top of the atmosphere and, most importantly, if and how the moisture in a particular region is affected by the moisture transported from neighboring regions. The composites were calculated for the domain by, first determining the P95 precipitation rate for each grid point; then determining all the precipitation rates greater than P95 precipitation to find the precipitation extreme events, such that each event can be denoted by $\mathbf{x}$.

Then, the mean of precipitation and other climatological variables associated with the precipitation extremes were determined to get a representative picture of the rate of precipitation. To calculate anomalies against wet days, the climatology of the variable for all wet days (i.e. days with precipitation greater than 1 mm/day) i.e. $\overline{\mathbf{x}}$, was calculated for each grid point. Then the composite anomaly for each climatological variable was determined by using the formula,

$$A = \overline{\mathbf{x} - \overline{\mathbf{x}}} \tag{7}$$

Then the analysis was repeated for all grid points, across the different dynamical and thermodynamic indices.

4 Results and Discussion

4.1 Apparent scaling of precipitation extreme over the Indian subcontinent

The apparent scaling rates, over the Indian subcontinent, for P95 precipitation against both DPT (shown in Fig. 2) and SAT (shown in supplementary Fig. S2) covariates. For the pre-monsoon season, the results highlight that the scaling rates against SAT covariates are consistently negative, except in the northern Bay of Bengal, northern parts of the Arabian Sea, and the Tibetan plateau (see region 1 in Fig. 1). Whereas for DPT, the scaling rates come to be positive throughout the domain, except in the offshore waters of Pakistan on the western side and south of the Andaman Sea (in the Indonesian offshore waters). Also, the negative scaling rates are more prominent, in the east Indian coast. The scaling rates are consistently found to be highly positive (negative) over the ocean than over the land against DPT (SAT) covariate. Over the ocean, the scaling rates are found to be greater than $42\%K^{-1}$ when using DPT as the scaling covariate, and the results are statistically significant at a 95% confidence, indicating that the precipitation intensities over the ocean respond much strongly to changes in temperatures than those over land. In a recent study, drawing from the results of a multimodel ensemble, Medeiros et al (2021) suggested a strong influence of the positive feedback due to cloud radiative effects (CREs) in strengthening the response of extreme precipitation over the tropical oceans. Precipitation over oceans occur largely due to organized convective systems such as tropical cyclones, Madden–Julian Oscillation (MJO) in the Indo-Pacific, equatorial waves, etc., and CREs are responsible in enhancing the organization of convection over the oceans (Medeiros et al, 2021). In the monsoon season, a zone of strong negative scaling against DPT covariate is apparent, extending from the east coast of the Indian landmass to the Bay of Bengal. This region of negative scaling is found in the southern Arabian Sea, southern Bay of Bengal and in just off the eastern coast of India. Moreover, negative scaling against DPT scaling covariate is also witnessed over regions of high orography, such as the Western Ghats, the foothills of the Himalayas in India; and the Arakan Mountains, Hengduan Mountains and the Tanasserim Hills in Myanmar (shown as regions 2, 4, 5 and 8 in Fig. 1). Also, strong positive scaling is observed in plateau regions, such as the Deccan Plateau in India and the Shan plateau (shown as region 7 in Fig. 1) in Myanmar. The thermodynamic response of extremes is largely negative over Bangladesh. Another interesting aspect is the highly positive scaling rates over the South-East Peninsular India (SEPI) region (9^oN - 15^oN; 77^oE - 81^oE; highlighted as region 3 in Fig. 1), which is generally termed as the rain-shadow region during the monsoon season due to being located on the lee-ward side of the Western Ghats. The cause of the high positive scaling can be largely attributed to the source of rainfall in these regions, which is largely caused by small scale convection due to the occurrence of isolated thunderstorms (a largely thermodynamically driven process) and, to a small extent, due to the sea-breeze circulation near the southeast coast (Mohan et al, 2021). For the apparent scaling results in the post-monsoon season, against the DPT scaling covariate, the scaling rates are found to be consistently positive throughout the domain, and again, the response of precipitation extremes over the ocean is found to be much higher than that over land.

The central tendencies, i.e. the median and mean scaling rates (against the DPT covariate) and associated standard deviations are summarized in Table 2, for all three seasons, to numerically highlight the seasonal changes in the overall scaling rates over the study region. The results clearly suggest that the scaling rates are lower during the ISM season, while the overall scaling rates are relatively higher and comparable during the pre-monsoon and post-monsoon season. These results are consistent with the findings from previous studies (Marelle et al, 2018; Williams and O'Gorman, 2022), which highlight, using model and observed precipitation data, that the fractional increase in precipitation extremes have been weaker during boreal summers rather than winters, suggesting a seasonal shift in precipitation extremes to later in the year, with strong future warming.

Table 2 Seasonal variations in the P95 median and mean apparent scaling rates (+/- standard deviation)

Season	Median Scaling Rates	Mean Scaling Rates (± std)
Pre-Monsoon	16.167	21.564 (±20.204)
Monsoon	8.149	7.958 (±27.708)
Post-Monsoon	17.648	25.919 (±21.239)

4.2 The seasonal changes in the thermodynamic and dynamic contribution to precipitation extremes

In order to probe into the probable causes in the deviations of apparent scaling rates from the expected climate scaling rate of $7\% K^{-1}$, it is important to

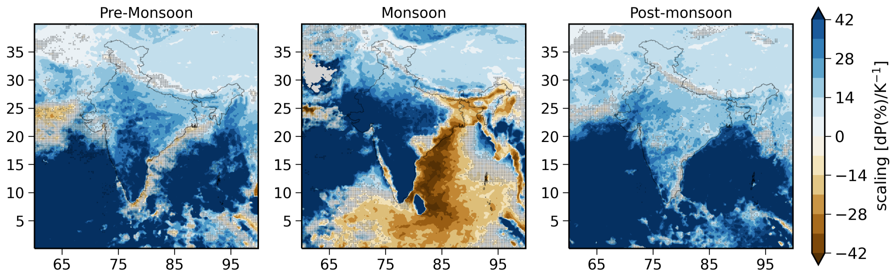

Fig. 2 Seasonal variations in apparent scaling rates of ERA5 daily P95 precipitation against DPT as a covariate. The stippling indicates grid-points without a 95% statistical significance. Here, x-axis represents longitude (^{o}E) and y-axis represents latitude (^{o}N).

analyze the characteristics of the precipitation extremes over the Indian subcontinent. The value of P95 at each grid point for the analysis period, across different seasons, was evaluated (shown in supplementary Fig. S3), and the extreme precipitation events at each grid point were selected as all the days with precipitation exceeding the P95 threshold valve at that grid point. Following the extraction of precipitation extremes at each grid point, the frequency of the extremes were computed to assess the number of daily extremes that occurred over the analysis period, for the three different seasons (shown in supplementary Fig. S4). The highest number of extremes are found in the monsoon season, with the regions of highest P95 values being mostly restricted to the Western Ghats, the foothills of the Himalayas and central India, with a small region in the head of the Arabian Sea receiving heavy precipitation, however the frequency of extremes in this region is very low. In the pre-monsoon season, the most number of the heaviest extremes occur, in the southern Bay of Bengal, and in the Himalayan foothills, and in the north-eastern states of India, and a similar pattern of extremes frequency is evident in the post-monsoon season. To better analyze the characteristics of extremes, the composites of precipitation extremes are plotted along with the composite anomaly of extremes against the wet days' climatology (see Fig. 3 top and middle rows)

In the pre-monsoon season, the highest intensity of extremes occur off the west coast of India, in the central part of the Arabian Sea, and in north and central Bay of Bengal off the east coast, and also in the north-eastern states of India. During the ISM, the heaviest extremes occur in the head of the Arabian Sea, in central India, foothills of the Himalayas, north-east of India, and in the Western Ghats. In the post-monsoon season, the heaviest extremes primarily occur in the East Coast and at the head of the Bay of Bengal, and in the foothills of the Himalayas and in the northern Arabian Sea. In all three seasons, high intensity daily extremes occur off the western coast of Indonesia.

To quantify the thermodynamic and dynamic contribution to the precipitation extremes, we investigated the absolute contribution to precipitation extremes due to dynamic factors (vertical transport of moist air due to large scale circulation) and thermodynamic factor (changes in local moisture content), using the scaling estimate technique discussed in section 3.2. In Fig. 3 bottom row, we compare the composites of the precipitation estimates,

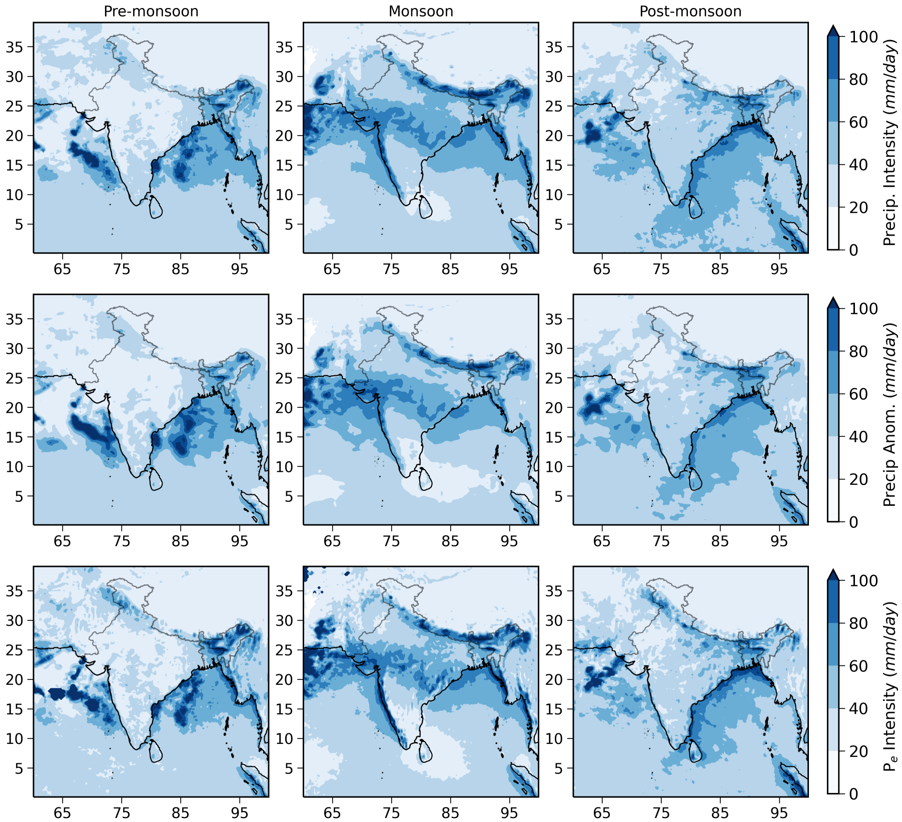

Fig. 3 Top: Composites of daily precipitation extremes across the three seasons. Middle: Composite anomaly of precipitation extremes (i.e. all events exceeding the P95 threshold) calculated against the climatology of wet days (i.e. all events with precipitation > 1 mm/-day) across the three different seasons. Bottom: Composites of the precipitation estimates determined using the scaling estimate technique across the three different seasons. Here, x-axis represents longitude (^{o}E) and y-axis represents latitude (^{o}N).

obtained using the scaling estimate technique, against the composites of ERA5 derived precipitation extremes (in the top row of the same figure), while the percentage bias is shown in supplementary Fig. S5. The percentage bias was calculated using formula shown in equation 8.

$$\% \, Bias = \frac{P_e - Precip}{Precip} \times 100 \tag{8}$$

The precipitation estimates show good agreement with the precipitation intensities in the reanalysis dataset, however, a mix of wet and dry bias is seen in regions of complex orography, while a large negative anomaly is seen in the Arabian Sea during the pre-monsoon season. But, overall the scaling estimate is able to capture the intensity and spatial distribution quite well which is further illustrated in Fig. 4 which highlights the kernel density distribution of the ERA5 derived precipitation extremes, associated precipitation estimate, *Dyn* and *Thermo* contribution, over the Indian subcontinent, across all three seasons.

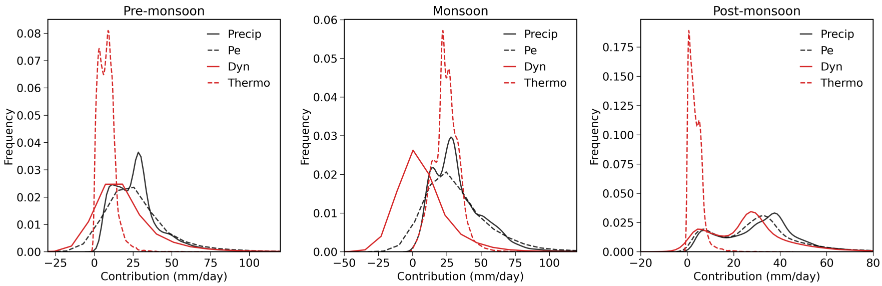

Fig. 4 Kernel density estimates of the spatial distribution of ERA5 derived precipitation extremes (Precip), associated precipitation estimate (P_e), *Dyn* and *Thermo* contribution, over the Indian subcontinent, during the pre-monsoon (left), monsoon (center) and post-monsoon (right) seasons.

The precipitation estimate was then decomposed into the dynamic and thermodynamic component, and the seasonal differences in the spatial distribution of the composites of dynamic and thermodynamic contribution to

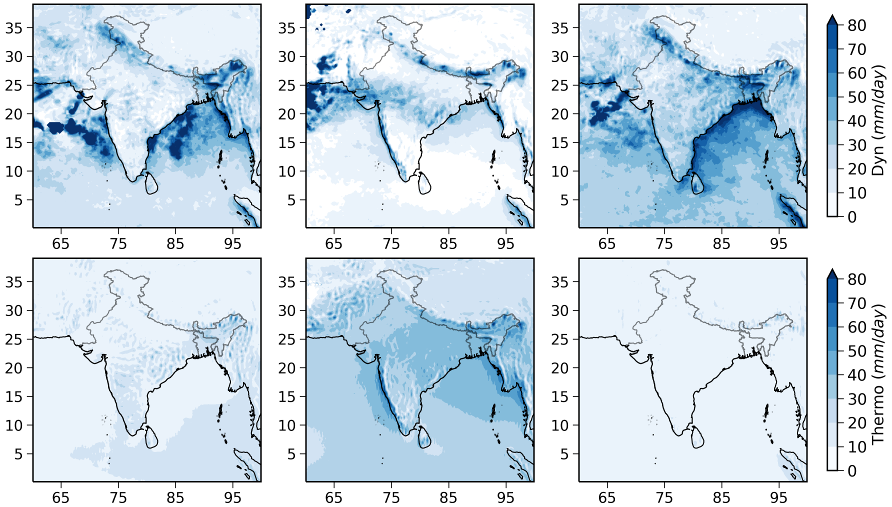

Fig. 5 Composites of Dynamic (top) and thermodynamic (bottom) contribution across all three seasons. Here, x-axis represents longitude (^{o}E) and y-axis represents latitude (^{o}N).

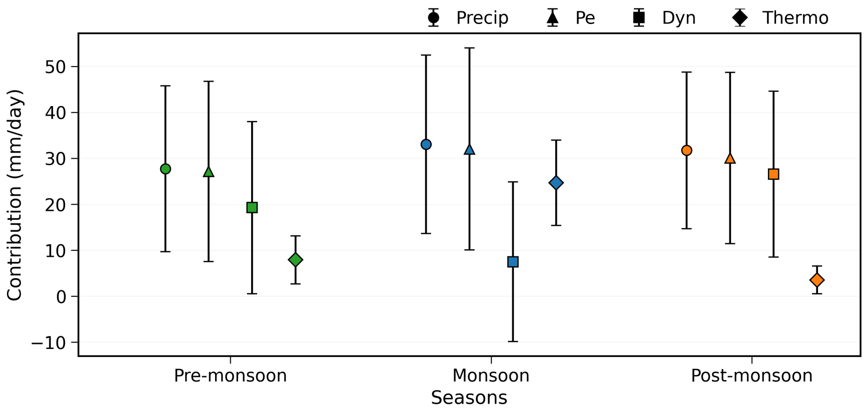

Fig. 6 Seasonal variation in mean precipitation extremes (Precip), associated precipitation scaling estimates (P_e), dynamic (*Dyn*) and thermodynamic (*Thermo*) contribution.

precipitation extremes is shown in the Fig. 5. From the results in Figs. 4 and 5, it is evident that the relative contribution of dynamic drivers over the thermodynamic drivers is highest during the pre-monsoon and post-monsoon seasons, while in the monsoon season, the thermodynamic drivers have a significantly higher relative contribution. However, if we consider only grid points having the highest intensity of extremes, the dynamic contribution is larger. To confirm these results, the mean value of the absolute contributions due to *Dyn* and *Thermo* (and the associated standard deviations) along with precipitation estimates were plotted in Fig. 6. Emori and Brown (2005) had also highlighted the significance of large scale dynamics in the tropics, and in continuation, Dairaku and Emori (2006), showed that the contribution of the dynamic component to extreme precipitation change exceeded the contribution to the thermodynamic component, especially over South Asian continental landmass. In a recent study, Sudharsan et al (2020) concluded that dynamic contribution to precipitation extremes plays an essential and crucial role in causing extreme precipitation events over India over an annual period. Hence the results of our analysis are in accordance with existing literature.

From the results, it is evident that first, the spatial distribution of precipitation scaling estimate closely matches the spatial distribution of the ERA5 derived extremes' intensities over the study region, and secondly, *Dyn* (*Thermo*) contribution is least (highest) during the monsoon season, while the opposite is true for the other two seasons. These results further strengthen the hypothesis that the weakened intensification of extreme during the boreal summer season, over the Northern Hemisphere, is due to weakened or suppressed vertical ascent (Marelle et al, 2018; Williams and O'Gorman, 2022).

4.3 Thermodynamic and dynamical features associated with precipitation extremes

To further probe into the causes and climatological drivers behind the lower dynamic contribution and elevated thermodynamic contribution in the monsoon season, we analyzed the composites and associated anomalies during precipitation extremes, for various climatological variables mentioned in section 2. Scaling of precipitation extremes is not just dependent on the precipitation intensities, but also on the temperature covariates used to estimate the scaling rates, namely DPT and SAT. Hence, we analyzed the DPT composites during extremes and composite anomalies against the climatology of wet days (see Fig. 7). A similar analysis was conducted for SAT (shown in supplementary Fig. S6). Majority of the grid points show negative SAT anomalies for extremes, and these grid points are associated with negative scaling rates when the SAT scaling covariate is used, while grid points with positive SAT anomalies are associated with positive precipitation-SAT scaling rates. This suggests that over the Indian subcontinent, the negative precipitation-SAT scaling rates can be largely attributed to a drop in SAT during extremes due to cooling associated with precipitation (Bao et al, 2018; Barbero et al, 2018; Lenderink et al, 2018)

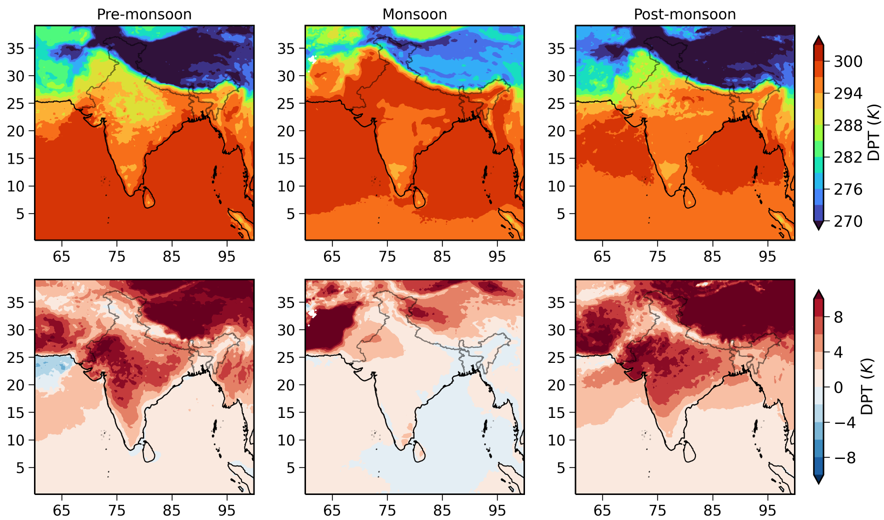

Fig. 7 Top: Composites of daily near surface DPT associated with extremes and, Bottom: Composite anomaly of DPT against the climatology of DPT on wet days (precipitation > 1 mm/day). Here, x-axis represents longitude (^{o}E) and y-axis represents latitude (^{o}N).

Moreover, we see predominantly positive SAT anomalies over the Tibetan plateau (shown as region 1 in Fig. 1), for all three seasons, which explains why we see consistently positive SAT scaling rates over this region, which are comparable to the DPT scaling rates. A previous study by Yong et al (2021) also highlighted that the DPT scaling rates in the Tibetan plateau are similar to the SAT scaling rates, and that the scaling rates are higher during the winter months compared to summer months, and similar results are found in our analysis. This is largely due to the occurrence of these extremes at SAT values higher than that normally found on wet days, which also highlights that higher temperatures do drive precipitation extremes, especially in climates that are generally colder, while humidity variations play a more important role in tropical and warmer climates. Also, seasonal variations in temperature play a huge role in the scaling rates.

Unlike the SAT anomalies, the DPT anomalies, during the extremes, are largely positive throughout the Indian subcontinent for all three seasons. But, in the monsoon season, the regions which were associated with negative DPT scaling rates also show negative DPT anomalies, highlighting that the precipitation extremes in these regions are associated with a dip in DPT values, which generally entails a dip in moisture availability and near surface humidity (Williams and O'Gorman, 2022). Moreover, the negative CAPE anomalies shown in the bottom row of Fig. 8, also highlight that extremes in these regions are generally associated with shallower convection as compared to other wet days, which could suggest that the extremes here are largely contributed by more dynamical factors, such as the transport of moisture from surrounding regions. Even in pre-monsoon and post-monsoon seasons, the grid points which were associated with negative scaling rates, are associated with negative

CAPE anomalies. This means that the extent of convection and upward movement of moist air in these regions must be largely dynamically driven, rather than being thermally driven. This further validates the findings of reduced Dyn contribution and weakened vertical ascent during the ISM.

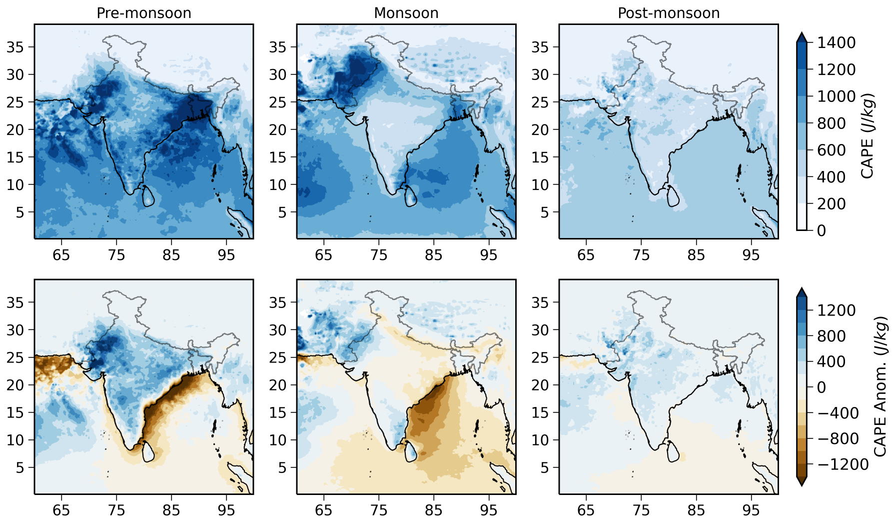

Fig. 8 Top: Composites of daily CAPE associated with extremes and, Bottom: Composite anomaly of CAPE against the climatology of CAPE on wet days (precipitation > 1 mm/day). Here, x-axis represents longitude (^{o}E) and y-axis represents latitude (^{o}N).

To further investigate the role of dynamical influence of large scale air circulation during extremes, we find the median and anomalies of Vertically Integrated Moisture Convergence (VIMC) and Vertically Integrated Moisture Transport (VIMT) which are shown in Figs. 9 and 10.

From the results, it is evident that the high intensity precipitation extremes in all three season occur largely due to convergence of moisture from remote areas due to the large scale circulation associated with the days of extremes, especially in regions where the precipitation intensity is greater than 70 mm/-day. The results of VIMT anomalies also highlight that the regions of the highest intensity extremes are associated with convergence of moisture and net

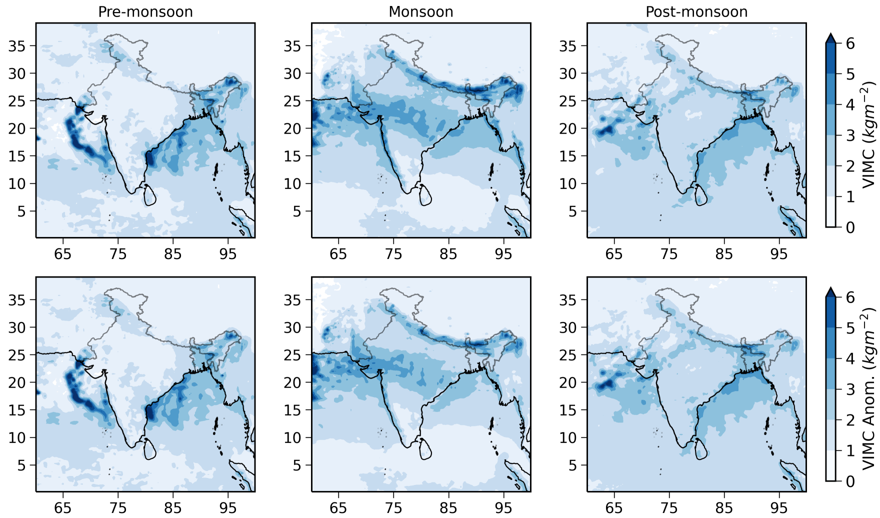

Fig. 9 Top: Composites of daily VIMC associated with extremes and, Bottom: Composite anomaly of VIMC against the climatology of VIMC on wet days (precipitation > 1 mm/day). Here, x-axis represents longitude (^{o}E) and y-axis represents latitude (^{o}N).

vertical transport of moist air. In the post-monsoon season, the extremes off the eastern coast, are largely caused by the south-easterly winds which occur primarily due to cyclonic storms which are the most active and intense during the post-monsoon season in the Bay of Bengal. These south-easterlies also cause extremes in the foothills of the Himalayas as well. In the monsoon season, the VIMT anomalies are mostly positive throughout the subcontinent, but have a small magnitude, which is largely due to the fact that VIMT for extremes doesn't show much difference than that during wet days, possibly suggesting that the dynamical driers causing heavy rainfall during monsoons season are the same as the ones causing light or moderate rainfall. The extremes in the Western Ghats are largely caused due to the south-westerlies and associated orographic lifting of the moisture-laden winds, while the extremes in central India are caused by the convergence of north-westerly and south-westerly winds flowing across the Indian subcontinent. Moreover, in the SEPI region, we see negative VIMT anomalies during the monsoons season, which suggests that the positive scaling rates in the region are largely driven by the positive CAPE anomalies, and the moisture laden westerlies are also a cause of extremes in the highlands of Myanmar. Similar results are highlighted in LLMT composites and associated anomalies (shown in supplementary Fig. S7).

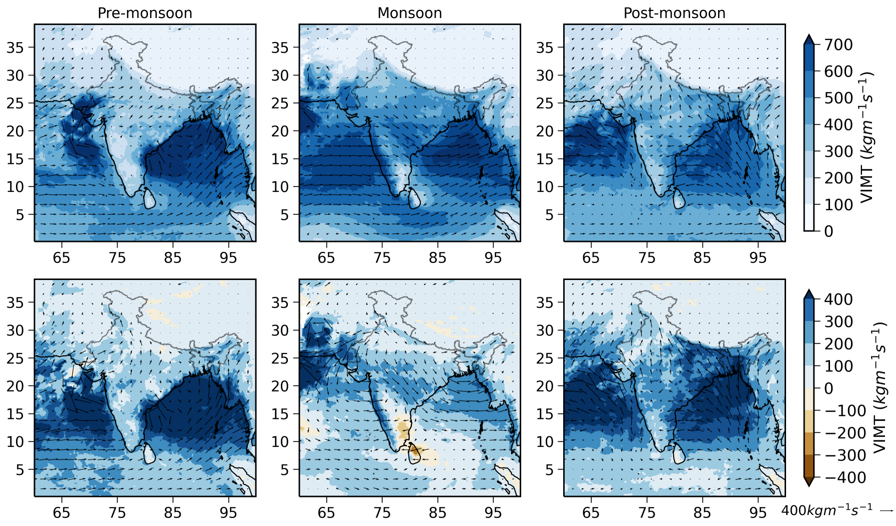

Fig. 10 Top: Composites of daily VIMT associated with extremes and, Bottom: Composite anomaly of VIMT against the climatology of VIMT on wet days (precipitation > 1 mm/day). Here, x-axis represents longitude (^{o}E) and y-axis represents latitude (^{o}N).

Hence, it is evident that positive (negative) DPT scaling rates are found in areas with positive (negative) DPT anomalies, and the negative DPT anomalies are largely due to negative CAPE anomalies during extremes which prevent the deep convection of moist air. Lower DPT temperatures also means lower availability of local low-level moisture, and coupled with shallower convection, we see rainfall extremes of relatively low intensity. This phenomenon is particularly evident in the monsoon season, where lower (higher) scaling rates were largely associated with lower (higher) CAPE and DPT anomalies as shown in Fig. 11, highlighting the zonal variation of apparent scaling (against DPT), CAPE anomalies and DPT anomalies during ISM. Similar conclusions can be drawn from the meridional variation of the same parameters during ISM (shown in supplementary Fig. S8). The heavier extremes are largely caused to transport of moisture from remote areas through the large scale air circulation and also due to the large scale convergence of moisture leading to strong upward movement of air, and also due to the lifting of air in regions of high orography. However, in the ISM season, the anomalies of the dynamical drivers are weaker, as compared to other two seasons, further validating the results obtained from the seasonal dip in *Dyn* contribution during monsoon season, shown in section 4.2. In summary, the regions of negative scaling rates are associated with either, negative CAPE anomalies, or with regions where large scale circulation and moisture transport dominate the role of local thermal factors and moisture availability, and the reduced dynamic contribution during summer ISM are largely associated with weak vertical ascent and lower near surface moisture availability, similar to the results found over much of the Northern Hemisphere (Williams and O'Gorman, 2022; Marelle et al, 2018). In a recent study, Huang et al (2021) studied the sensitivity of hourly extremes over Eastern China, and found negative scaling rates above a certain threshold temperature and also attributed these to a suppressed convection, driven by increase in Convective Inhibition (CIN) at higher temperatures. We find similar results and a similar driving mechanism over India during the monsoon season. But, in the pre-monsoon and post-monsoon seasons, the heaviest extremes are driven primarily due to moisture convection and vertical transport of moisture, with high values of low level moisture availability and high CAPE anomalies driving the convection of moisture laden air upwards, causing deep convection of moist air leading to rise in the intensity of extremes, and high sensitivity to increasing temperatures.

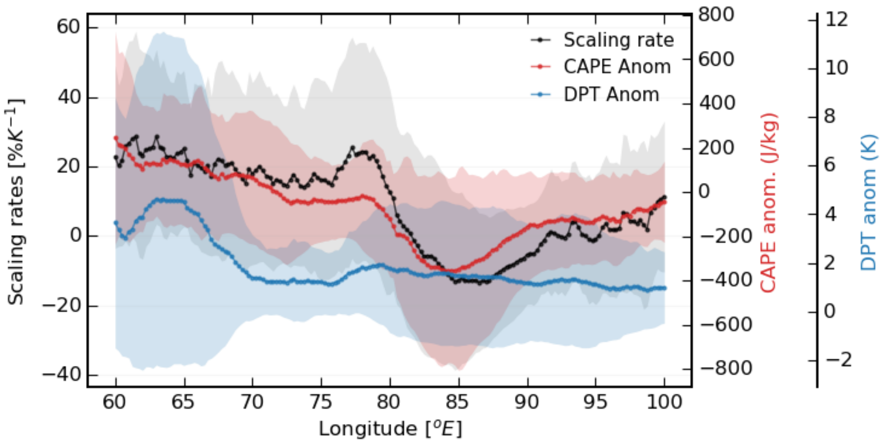

Fig. 11 Zonal variation of apparent scaling rates, CAPE anomalies, and DPT anomalies during precipitation extremes over the Indian subcontinent, during the Indian summer monsoon season. The shaded regions represent the standard deviations associated with spatial distribution.

5 Conclusions

Rainfall extremes are rising and will continue to rise over the Indian subcontinent, and they pose a serious threat to the geographical and socio-economical integrity of the region. Several studies had been done to understand the variability in the intensity and frequency of extremes, with changing temperatures in a warming climate, and also for understanding the physical drivers behind them. But, a detailed analysis of these seasonal changes in the sensitivity of precipitation extremes to changing temperatures, as well as the dynamical and thermodynamic linkages associated with these seasonal changes was lacking, especially over the Indian subcontinent region, which is home to a large percentage of the world population and highly prone to potential damages linked with extremes driven flash floods and debris flow. So, we attempted to determine these seasonal variations in scaling rates and probable dynamical and thermodynamic drivers causing these variations, over the subcontinent.

Apparent scaling rates are found to be higher for post-monsoon season, followed by pre-monsoon season, and least for monsoon seasons. Significantly lower and mostly negative scaling rates are observed over large parts of the Indian subcontinent when estimating the rates against the SAT covariate, across all seasons. On the other hand, the scaling rates are higher and more consistently positive when using the DPT covariate for scaling purposes. Only the Tibetan plateau showed consistently positive scaling rates against SAT, across all three seasons. The scaling rates were also found to be higher over the ocean, than over land, consistent with previous studies.

Significant deviations from the expected CC scaling are observed across all three seasons, and to probe into the causes behind these deviations, we decomposed precipitation intensity to its dynamic and thermodynamic contribution. The dynamic contribution to precipitation extremes is found to dominate in the post-monsoon season, followed by the pre-monsoon season, however the thermodynamic contribution dominates in the monsoon season, while the dynamic contribution is lower comparatively.

To validate these results, the seasonal differences in the climatological drivers during extremes was analyzed, and it is found that the scaling rates over the Tibetan plateau were positive against both SAT and DPT since both SAT and DPT increase during days of the extreme event occurrence when compared against all wet days. This highlights that higher temperatures do drive more intense extremes, especially in climate that are generally cooler, while humidity variations play a more important role in tropical and warmer climates.

The negative scaling rates can be largely attributed to negative CAPE anomalies and negative DPT anomalies leading to lower moisture availability and energy for deep convection, and reduced precipitation intensities for extremes. This is especially true in the monsoon season, further validating the dip in the dynamic contribution to extremes during the monsoon season.

Furthermore, in regions of high orography, the negative scaling rates can be largely attributed to the predominant effect of dynamic factors such as transport of moisture from remote areas and moisture convergence due to the large scale circulation associated with extremes. So in some regions, dynamic influence causes enhancement of scaling rates, such as over central India (during the monsoon season), or in the east coast and foothills of the Himalayas (during the post-monsoon season), due to cyclonic storms bringing moisture laden winds from the Bay of Bengal. While, in regions of high orography, dynamic influence also causes lower/negative scaling rates, because the assisted convection due to orographic lifting causes saturation even at lower dew point temperatures and thus the intensification of extremes is not highlighted in the apparent scaling rates.

The super-CC scaling rates can also be attributed to the high positive CAPE anomalies associated with latent heat release due to higher DPT values and local moisture availability, causing conditional instability and deeper convection, leading to increase in scaling rates beyond the expected climate scaling. An example of this can be found in the case of SEPI, where we find positive scaling rates during the monsoon season, despite negative VIMT and VIMC anomalies. In SEPI, the extremes occur largely due to thunderstorm activities.

Overall, it can be concluded that seasonal changes in near surface air temperature and dew point temperature, CAPE and large scale circulation significantly influence the spatial distribution of apparent scaling rates, and also influence the magnitude of the scaling rates, particularly during the summer monsoon season, primarily by weakening of dynamical influences. The results of the present study, provide a better understanding of the drivers of precipitation extremes over the Indian subcontinent, and sheds light on the variations in these drivers across the different seasons. Further research can be done to analyze and attribute these drivers to anthropogenic warming scenarios using general circulation models such as CMIP6, or even using regional climate models, to further probe into how these dynamical and thermodynamic drivers will change in the near and far future climate projections, under different warming scenarios. This will help in improving the fidelity of the climate projections of average and extreme precipitation in the regional climate models (RCMs), and, in turn, help provide insights to climatologists as well as climate policy-makers about the long-term changes in the intensity and frequency of precipitation extremes at a regional level.

Statements and Declarations

Acknowledgment

The authors would like to acknowledge ECMWF for making available the ERA5 reanalysis climatological variables on single levels and different pressure levels.

Funding

The authors declare that no funds, grants, or other support were received during the preparation of this manuscript.

Competing Interests

Corresponding author declares on behalf of all the authors, there is no competing interest that influence the outcome reported in this manuscript.

Author Contributions

Aditya Sengupta: Analysis and interpretation the results, writing, editing the original draft. **Naresh Krishna Vissa:** Supervision, conceptualization and writing and reviewing the original draft. **Indrani Roy:** Interpretation of the results, reviewing and editing the original draft.

Data Availability

Data relevant to the paper can be downloaded from the following websites. ERA5 precipitation and temperature data on single levels :
https://cds.climate.copernicus.eu/cdsapp#!/dataset/reanalysis-era5-single-levels,
ERA5 data on pressure levels - https://cds.climate.copernicus.eu/cdsapp#!/dataset/reanalysis-era5-pressure-levels.

References

Alexander LV (2016) Global observed long-term changes in temperature and precipitation extremes: A review of progress and limitations in IPCC assessments and beyond. Weather and Climate Extremes 11:4–16. https://doi.org/10.1016/j.wace.2015.10.007, URL https://linkinghub.elsevier.com/retrieve/pii/S2212094715300414

Ali H, Mishra V (2017) Contrasting response of rainfall extremes to increase in surface air and dewpoint temperatures at urban locations in India. Scientific Reports 7(1):1228. https://doi.org/10.1038/s41598-017-01306-1, URL http://www.nature.com/articles/s41598-017-01306-1

Ali H, Mishra V (2018a) Contributions of Dynamic and Thermodynamic Scaling in Subdaily Precipitation Extremes in India. Geophysical Research Letters 45(5):2352–2361. https://doi.org/10.1002/2018GL077065, URL https://onlinelibrary.wiley.com/doi/abs/10.1002/2018GL077065

Ali H, Mishra V (2018b) Increase in Subdaily Precipitation Extremes in India Under 1.5 and 2.0 °C Warming Worlds. Geophysical Research Letters 45(14):6972–6982. https://doi.org/10.1029/2018GL078689, URL https://onlinelibrary.wiley.com/doi/abs/10.1029/2018GL078689

Ali H, Fowler HJ, Mishra V (2018) Global Observational Evidence of Strong Linkage Between Dew Point Temperature and Precipitation Extremes. Geophysical Research Letters 45(22):12,320–12,330. https://doi.org/10.1029/2018GL080557, URL https://onlinelibrary.wiley.com/doi/abs/10.1029/2018GL080557

Ali H, Fowler HJ, Lenderink G, et al (2021a) Consistent Large-Scale Response of Hourly Extreme Precipitation to Temperature Variation Over Land. Geophysical Research Letters 48(4). https://doi.org/10.1029/2020GL090317, URL https://onlinelibrary.wiley.com/doi/10.1029/2020GL090317

Ali H, Peleg N, Fowler HJ (2021b) Global Scaling of Rainfall With Dewpoint Temperature Reveals Considerable Ocean-Land Difference. Geophysical Research Letters 48(15). https://doi.org/10.1029/2021GL093798, URL https://onlinelibrary.wiley.com/doi/10.1029/2021GL093798

Allan RP, Soden BJ (2008) Atmospheric Warming and the Amplification of Precipitation Extremes. Science 321(5895):1481–1484. https://doi.org/10.1126/science.1160787, URL https://www.science.org/doi/10.1126/science.1160787

Anandh PC, Vissa NK (2020) On the linkage between extreme rainfall and the Madden–Julian Oscillation over the Indian region. Meteorological Applications 27(2):e1901. https://doi.org/10.1002/met.1901, URL https://onlinelibrary.wiley.com/doi/abs/10.1002/met.1901, _eprint:

https://onlinelibrary.wiley.com/doi/pdf/10.1002/met.1901

Bao J, Sherwood SC, Alexander LV, et al (2017) Future increases in extreme precipitation exceed observed scaling rates. Nature Climate Change 7(2):128–132. https://doi.org/10.1038/nclimate3201, URL http://www.nature.com/articles/nclimate3201

Bao J, Sherwood SC, Alexander LV, et al (2018) Comments on "temperature-extreme precipitation scaling: A two-way causality?". International Journal of Climatology 38(12):4661–4663. https://doi.org/10.1002/joc.5665, URL https://onlinelibrary.wiley.com/doi/10.1002/joc.5665

Barbero R, Westra S, Lenderink G, et al (2018) Temperature-extreme precipitation scaling: a two-way causality? International Journal of Climatology 38(S1). https://doi.org/10.1002/joc.5370, URL https://onlinelibrary.wiley.com/doi/10.1002/joc.5370

Bhattacharyya S, Sreekesh S, King A (2022) Characteristics of extreme rainfall in different gridded datasets over India during 1983–2015. Atmospheric Research 267:105,930. https://doi.org/10.1016/j.atmosres.2021.105930, URL https://linkinghub.elsevier.com/retrieve/pii/S0169809521004865

Blenkinsop S, Chan SC, Kendon EJ, et al (2015) Temperature influences on intense UK hourly precipitation and dependency on large-scale circulation. Environmental Research Letters 10(5):054,021. https://doi.org/10.1088/1748-9326/10/5/054021, URL https://doi.org/10.1088/1748-9326/10/5/054021, publisher: IOP Publishing

Chen W, Cui H, Ge Q (2022) The spatial and seasonal dependency of daily precipitation extremes on the temperature in China from 1957 to 2017.

International Journal of Climatology 42(3):1560–1575. https://doi.org/10.1002/joc.7320, URL https://onlinelibrary.wiley.com/doi/10.1002/joc.7320

Dairaku K, Emori S (2006) Dynamic and thermodynamic influences on intensified daily rainfall during the Asian summer monsoon under doubled atmospheric CO $_2$ conditions: INTENSIFIED EXTREME ASIAN MONSOON. Geophysical Research Letters 33(1):n/a–n/a. https://doi.org/10.1029/2005GL024754, URL http://doi.wiley.com/10.1029/2005GL024754

Dimri AP (2013) Intraseasonal oscillation associated with the Indian winter monsoon. Journal of Geophysical Research: Atmospheres 118(3):1189–1198. https://doi.org/10.1002/jgrd.50144, URL https://onlinelibrary.wiley.com/doi/abs/10.1002/jgrd.50144, _eprint: https://onlinelibrary.wiley.com/doi/pdf/10.1002/jgrd.50144

Emori S, Brown SJ (2005) Dynamic and thermodynamic changes in mean and extreme precipitation under changed climate: MEAN AND EXTREME PRECIPITATION CHANGES. Geophysical Research Letters 32(17). https://doi.org/10.1029/2005GL023272, URL http://doi.wiley.com/10.1029/2005GL023272

Evan AT, Camargo SJ (2011) A Climatology of Arabian Sea Cyclonic Storms. Journal of Climate 24(1):140–158. https://doi.org/10.1175/2010JCLI3611.1, URL https://journals.ametsoc.org/view/journals/clim/24/1/2010jcli3611.1.xml, publisher: American Meteorological Society Section: Journal of Climate

Fadhel S, Rico-Ramirez MA, Han D (2018) Sensitivity of peak flow to the change of rainfall temporal pattern due to warmer climate. Journal of Hydrology 560:546–559. https://doi.org/10.1016/j.jhydrol.2018.03.041, URL https://linkinghub.elsevier.com/retrieve/pii/S0022169418302075

Fischer EM, Knutti R (2016) Observed heavy precipitation increase confirms theory and early models. Nature Climate Change 6(11):986–991. https://doi.org/10.1038/nclimate3110, URL http://www.nature.com/articles/nclimate3110

Fowler HJ, Lenderink G, Prein AF, et al (2021) Anthropogenic intensification of short-duration rainfall extremes. Nature Reviews Earth & Environment 2(2):107–122. https://doi.org/10.1038/s43017-020-00128-6, URL http://www.nature.com/articles/s43017-020-00128-6

Francis PA, Gadgil S (2006) Intense rainfall events over the west coast of India. Meteorology and Atmospheric Physics 94(1):27–42. https://doi.org/10.1007/s00703-005-0167-2, URL https://doi.org/10.1007/s00703-005-0167-2

Groisman PY, Knight RW, Easterling DR, et al (2005) Trends in Intense Precipitation in the Climate Record. Journal of Climate 18(9):1326–1350. https://doi.org/10.1175/JCLI3339.1, URL http://journals.ametsoc.org/doi/10.1175/JCLI3339.1

Guerreiro SB, Fowler HJ, Barbero R, et al (2018) Detection of continental-scale intensification of hourly rainfall extremes. Nature Climate Change 8(9):803–807. https://doi.org/10.1038/s41558-018-0245-3, URL http://www.nature.com/articles/s41558-018-0245-3

Hamada A, Murayama Y, Takayabu YN (2014) Regional Characteristics of Extreme Rainfall Extracted from TRMM PR Measurements. Journal of Climate 27(21):8151–8169. https://doi.org/10.1175/JCLI-D-14-00107.1, URL https://journals.ametsoc.org/view/journals/clim/27/21/jcli-d-14-00107.1.

xml, publisher: American Meteorological Society Section: Journal of Climate

Hardwick Jones R, Westra S, Sharma A (2010) Observed relationships between extreme sub-daily precipitation, surface temperature, and relative humidity: RELATIONSHIP BETWEEN PRECIP, TEMP, AND RH. Geophysical Research Letters 37(22):n/a–n/a. https://doi.org/10.1029/2010GL045081, URL http://doi.wiley.com/10.1029/2010GL045081

Herath SM, Sarukkalige R, Nguyen VTV (2018) Evaluation of empirical relationships between extreme rainfall and daily maximum temperature in Australia. Journal of Hydrology 556:1171–1181. https://doi.org/10.1016/j.jhydrol.2017.01.060, URL https://linkinghub.elsevier.com/retrieve/pii/S0022169417300690

Hersbach H, Bell B, Berrisford P, et al (2020) The ERA5 global reanalysis. Quarterly Journal of the Royal Meteorological Society 146(730):1999–2049. https://doi.org/10.1002/qj.3803, URL https://onlinelibrary.wiley.com/doi/abs/10.1002/qj.3803, _eprint: https://onlinelibrary.wiley.com/doi/pdf/10.1002/qj.3803

Hosseini-Moghari SM, Sun S, Tang Q, et al (2022) Scaling of precipitation extremes with temperature in China's mainland: Evaluation of satellite precipitation data. Journal of Hydrology 606:127,391. https://doi.org/10.1016/j.jhydrol.2021.127391, URL https://linkinghub.elsevier.com/retrieve/pii/S0022169421014414

Huang D, Zhu J, Xiao X, et al (2021) Understanding the sensitivity of hourly precipitation extremes to the warming climate over Eastern China. Environmental Research Communications 3(8):081,002. https://doi.org/10.1088/2515-7620/ac17e1, URL https://doi.org/10.1088/2515-7620/ac17e1, publisher: IOP Publishing

Kharin VV, Zwiers FW, Zhang X, et al (2013) Changes in temperature and precipitation extremes in the CMIP5 ensemble. Climatic Change 119(2):345–357. https://doi.org/10.1007/s10584-013-0705-8, URL http://link.springer.com/10.1007/s10584-013-0705-8

Kikuchi K, Wang B (2010) Formation of Tropical Cyclones in the Northern Indian Ocean Associated with Two Types of Tropical Intraseasonal Oscillation Modes. Journal of the Meteorological Society of Japan Ser II 88(3):475–496. https://doi.org/10.2151/jmsj.2010-313

Krishnamurthy V, Ajayamohan RS (2010) Composite Structure of Monsoon Low Pressure Systems and Its Relation to Indian Rainfall. Journal of Climate 23(16):4285–4305. https://doi.org/10.1175/2010JCLI2953.1, URL https://journals.ametsoc.org/view/journals/clim/23/16/2010jcli2953.1.xml, publisher: American Meteorological Society Section: Journal of Climate

Kumari A, Kumar P, Dubey AK, et al (2021) Dynamical and thermodynamical aspects of precipitation events over India. International Journal of Climatology p joc.7409. https://doi.org/10.1002/joc.7409, URL https://onlinelibrary.wiley.com/doi/10.1002/joc.7409

Lélé MI, Leslie LM, Lamb PJ (2015) Analysis of low-level atmospheric moisture transport associated with the west african monsoon. Journal of Climate 28(11):4414–4430. https://doi.org/10.1175/jcli-d-14-00746.1, URL https://doi.org/10.1175%2Fjcli-d-14-00746.1

Lenderink G, van Meijgaard E (2008) Increase in hourly precipitation extremes beyond expectations from temperature changes. Nature Geoscience 1(8):511–514. https://doi.org/10.1038/ngeo262, URL http://www.nature.com/articles/ngeo262

Lenderink G, Barbero R, Loriaux JM, et al (2017) Super-Clausius–Clapeyron Scaling of Extreme Hourly Convective Precipitation and Its Relation to Large-Scale Atmospheric Conditions. Journal of Climate 30(15):6037–6052. https://doi.org/10.1175/JCLI-D-16-0808.1, URL https://journals.ametsoc.org/doi/10.1175/JCLI-D-16-0808.1

Lenderink G, Barbero R, Westra S, et al (2018) Reply to comments on “Temperature-extreme precipitation scaling: a two-way causality?”. International Journal of Climatology 38(12):4664–4666. https://doi.org/10.1002/joc.5799, URL https://onlinelibrary.wiley.com/doi/10.1002/joc.5799

Liang W, Zhang M (2021) Summer and winter precipitation in East Asia scale with global warming at different rates. Communications Earth & Environment 2(1):150. https://doi.org/10.1038/s43247-021-00219-2, URL http://www.nature.com/articles/s43247-021-00219-2

Liu B, Tan X, Gan TY, et al (2020) Global atmospheric moisture transport associated with precipitation extremes: Mechanisms and climate change impacts. WIREs Water 7(2). https://doi.org/10.1002/wat2.1412, URL https://onlinelibrary.wiley.com/doi/10.1002/wat2.1412

Magan B, Kim S, Wasko C, et al (2020) Impact of atmospheric circulation on the rainfall-temperature relationship in Australia. Environmental Research Letters 15(9):094,098. https://doi.org/10.1088/1748-9326/abab35, URL https://iopscience.iop.org/article/10.1088/1748-9326/abab35

Mahto SS, Mishra V (2019) Does ERA-5 Outperform Other Reanalysis Products for Hydrologic Applications in India? Journal of Geophysical Research: Atmospheres 124(16):9423–9441. https://doi.org/10.1029/2019JD031155, URL https://onlinelibrary.wiley.com/doi/10.1029/2019JD031155

Marelle L, Myhre G, Hodnebrog Ø, et al (2018) The changing seasonality of extreme daily precipitation. Geophysical Research Letters 45(20):11–352

Medeiros B, Clement AC, Benedict JJ, et al (2021) Investigating the impact of cloud-radiative feedbacks on tropical precipitation extremes. npj Climate and Atmospheric Science 4(1):1–10. https://doi.org/10.1038/s41612-021-00174-x, URL https://www.nature.com/articles/s41612-021-00174-x, number: 1 Publisher: Nature Publishing Group

Mishra V, Smoliak BV, Lettenmaier DP, et al (2012) A prominent pattern of year-to-year variability in Indian Summer Monsoon Rainfall. Proceedings of the National Academy of Sciences 109(19):7213–7217. https://doi.org/10.1073/pnas.1119150109, URL https://www.pnas.org/doi/full/10.1073/pnas.1119150109, publisher: Proceedings of the National Academy of Sciences

Mohan T, Kumar KN, Madhulatha A, et al (2021) Intriguing aspects of rainfall initiation over rainshadow region during boreal summer monsoon. Atmospheric Research 261:105,746. https://doi.org/10.1016/j.atmosres.2021.105746, URL https://linkinghub.elsevier.com/retrieve/pii/S0169809521003021

Mohanty UC, Osuri KK, Pattanayak S, et al (2012) An observational perspective on tropical cyclone activity over Indian seas in a warming environment. Natural Hazards 63(3):1319–1335. https://doi.org/10.1007/s11069-011-9810-z, URL https://doi.org/10.1007/s11069-011-9810-z

Moustakis Y, Onof CJ, Paschalis A (2020) Atmospheric convection, dynamics and topography shape the scaling pattern of hourly rainfall extremes with temperature globally. Communications Earth & Environment 1(1):11. https://doi.org/10.1038/s43247-020-0003-0, URL https://www.nature.com/articles/s43247-020-0003-0

Mukherjee S, Aadhar S, Stone D, et al (2018) Increase in extreme precipitation events under anthropogenic warming in India. Weather and Climate Extremes 20:45–53. https://doi.org/10.1016/j.wace.2018.03.005, URL https://linkinghub.elsevier.com/retrieve/pii/S2212094717301068

Myhre G, Alterskjær K, Stjern CW, et al (2019) Frequency of extreme precipitation increases extensively with event rareness under global warming. Scientific reports 9(1):1–10

Nayak S (2018) Do Extreme Precipitation Intensities Linked to Temperature Over India Follow the Clausius–Clapeyron Relationship? Current Science 115(3):391. https://doi.org/10.18520/cs/v115/i3/391-392, URL https://www.currentscience.ac.in/Volumes/115/03/0391.pdf

O'Gorman PA, Schneider T (2009) The physical basis for increases in precipitation extremes in simulations of 21st-century climate change. Proceedings of the National Academy of Sciences 106(35):14,773–14,777. https://doi.org/10.1073/pnas.0907610106, URL https://pnas.org/doi/full/10.1073/pnas.0907610106

Oueslati B, Yiou P, Jézéquel A (2019) Revisiting the dynamic and thermodynamic processes driving the record-breaking January 2014 precipitation in the southern UK. Scientific Reports 9(1):2859. https://doi.org/10.1038/s41598-019-39306-y, URL http://www.nature.com/articles/

s41598-019-39306-y

Ougahi JH, Mahmood SA (2022) Evaluation of satellite-based and reanalysis precipitation datasets by hydrologic simulation in the Chenab river basin. Journal of Water and Climate Change 13(3):1563–1582. https://doi.org/10.2166/wcc.2022.410, URL https://iwaponline.com/jwcc/article/13/3/1563/86339/Evaluation-of-satellite-based-and-reanalysis

O'Gorman PA (2015) Precipitation Extremes Under Climate Change. Current Climate Change Reports 1(2):49–59. https://doi.org/10.1007/s40641-015-0009-3, URL http://link.springer.com/10.1007/s40641-015-0009-3

O'Gorman PA, Schneider T (2009) Scaling of Precipitation Extremes over a Wide Range of Climates Simulated with an Idealized GCM. Journal of Climate 22(21):5676–5685. https://doi.org/10.1175/2009JCLI2701.1, URL http://journals.ametsoc.org/doi/10.1175/2009JCLI2701.1

Papalexiou SM, Montanari A (2019) Global and Regional Increase of Precipitation Extremes under Global Warming. Water Resources Research p 2018WR024067. https://doi.org/10.1029/2018WR024067, URL https://onlinelibrary.wiley.com/doi/abs/10.1029/2018WR024067

Park IH, Min SK (2017) Role of Convective Precipitation in the Relationship between Subdaily Extreme Precipitation and Temperature. Journal of Climate 30(23):9527–9537. https://doi.org/10.1175/JCLI-D-17-0075.1, URL https://journals.ametsoc.org/doi/10.1175/JCLI-D-17-0075.1

Pattanaik DR, Rajeevan M (2010) Variability of extreme rainfall events over India during southwest monsoon season: ANALYSIS OF EXTREME RAINFALL EVENTS DURING JJAS. Meteorological Applications 17(1):88–104. https://doi.org/10.1002/met.164, URL https://onlinelibrary.wiley.com/doi/10.1002/met.164

Pfahl S, O'Gorman PA, Fischer EM (2017) Understanding the regional pattern of projected future changes in extreme precipitation. Nature Climate Change 7(6):423–427. https://doi.org/10.1038/nclimate3287, URL http://www.nature.com/articles/nclimate3287

Romatschke U, Medina S, Houze RA (2010) Regional, Seasonal, and Diurnal Variations of Extreme Convection in the South Asian Region. Journal of Climate 23(2):419–439. https://doi.org/10.1175/2009JCLI3140.1, URL https://journals.ametsoc.org/view/journals/clim/23/2/2009jcli3140.1.xml, publisher: American Meteorological Society Section: Journal of Climate

Roxy MK, Ghosh S, Pathak A, et al (2017) A threefold rise in widespread extreme rain events over central India. Nature Communications 8(1):708. https://doi.org/10.1038/s41467-017-00744-9, URL https://www.nature.com/articles/s41467-017-00744-9, number: 1 Publisher: Nature Publishing Group

Saha U, Sateesh M (2022) Rainfall extremes on the rise: Observations during 1951–2020 and bias-corrected CMIP6 projections for near- and late 21st century over Indian landmass. Journal of Hydrology 608:127,682. https://doi.org/10.1016/j.jhydrol.2022.127682, URL https://www.sciencedirect.com/science/article/pii/S0022169422002578

Sudharsan N, Karmakar S, Fowler HJ, et al (2020) Large-scale dynamics have greater role than thermodynamics in driving precipitation extremes over India. Climate Dynamics 55(9-10):2603–2614. https://doi.org/10.1007/s00382-020-05410-3, URL https://link.springer.com/10.1007/s00382-020-05410-3

Trenberth KE, Dai A, Rasmussen RM, et al (2003) The Changing Character of Precipitation. Bulletin of the American Meteorological Society 84(9):1205–1218. https://doi.org/10.1175/BAMS-84-9-1205, URL https://journals.ametsoc.org/doi/10.1175/BAMS-84-9-1205

Tyagi B, Naresh Krishna V, Satyanarayana ANV (2011) Study of thermodynamic indices in forecasting pre-monsoon thunderstorms over Kolkata during STORM pilot phase 2006–2008. Natural Hazards 56(3):681–698. https://doi.org/10.1007/s11069-010-9582-x, URL https://doi.org/10.1007/s11069-010-9582-x

Utsumi N, Seto S, Kanae S, et al (2011) Does higher surface temperature intensify extreme precipitation?: TEMPERATURE AND EXTREME RAINFALL. Geophysical Research Letters 38(16):n/a–n/a. https://doi.org/10.1029/2011GL048426, URL http://doi.wiley.com/10.1029/2011GL048426

Virts KS, Houze RA (2016) Seasonal and Intraseasonal Variability of Mesoscale Convective Systems over the South Asian Monsoon Region. Journal of the Atmospheric Sciences 73(12):4753–4774. https://doi.org/10.1175/JAS-D-16-0022.1, URL https://journals.ametsoc.org/view/journals/atsc/73/12/jas-d-16-0022.1.xml, publisher: American Meteorological Society Section: Journal of the Atmospheric Sciences

Vissa NK, Satyanarayana ANV, Prasad Kumar B (2013) Intensity of tropical cyclones during pre- and post-monsoon seasons in relation to accumulated tropical cyclone heat potential over Bay of Bengal. Natural Hazards 68(2):351–371. https://doi.org/10.1007/s11069-013-0625-y, URL https://doi.org/10.1007/s11069-013-0625-y

Vittal H, Ghosh S, Karmakar S, et al (2016) Lack of Dependence of Indian Summer Monsoon Rainfall Extremes on Temperature: An Observational Evidence. Scientific Reports 6(1):31,039. https://doi.org/10.1038/srep31039, URL http://www.nature.com/articles/srep31039

Wang Z, Duan A, Yang S, et al (2017) Atmospheric moisture budget and its regulation on the variability of summer precipitation over the Tibetan Plateau: TP Moisture Budget and Precipitation. Journal of Geophysical Research: Atmospheres 122(2):614–630. https://doi.org/10.1002/2016JD025515, URL http://doi.wiley.com/10.1002/2016JD025515

Wasko C, Lu WT, Mehrotra R (2018) Relationship of extreme precipitation, dry-bulb temperature, and dew point temperature across Australia. Environmental Research Letters 13(7):074,031. https://doi.org/10.1088/1748-9326/aad135, URL https://iopscience.iop.org/article/10.1088/1748-9326/aad135

Westra S, Alexander LV, Zwiers FW (2013) Global Increasing Trends in Annual Maximum Daily Precipitation. Journal of Climate 26(11):3904–3918. https://doi.org/10.1175/JCLI-D-12-00502.1, URL http://journals.ametsoc.org/doi/10.1175/JCLI-D-12-00502.1

Westra S, Fowler HJ, Evans JP, et al (2014) Future changes to the intensity and frequency of short-duration extreme rainfall: FUTURE INTENSITY OF SUB-DAILY RAINFALL. Reviews of Geophysics 52(3):522–555. https://doi.org/10.1002/2014RG000464, URL http://doi.wiley.com/10.1002/2014RG000464

Williams AIL, O'Gorman PA (2022) Summer-Winter Contrast in the Response of Precipitation Extremes to Climate Change Over Northern Hemisphere Land. Geophysical Research Letters 49(10):e2021GL096,531. https://doi.org/10.1029/2021GL096531, URL https://onlinelibrary.wiley.com/doi/abs/10.1029/2021GL096531, _eprint: https://onlinelibrary.wiley.com/doi/pdf/10.1029/2021GL096531

Yamada TJ, Hoshino T, Suzuki A (2021) Using a massive high-resolution ensemble climate data set to examine dynamic and thermodynamic aspects of heavy precipitation change. Atmospheric Science Letters 22(12). https://doi.org/10.1002/asl.1065, URL https://onlinelibrary.wiley.com/doi/10.1002/asl.1065

Yang Z, Dominguez F (2019) Investigating Land Surface Effects on the Moisture Transport over South America with a Moisture Tagging Model. Journal of Climate 32(19):6627–6644. https://doi.org/10.1175/JCLI-D-18-0700.1, URL https://journals.ametsoc.org/view/journals/clim/32/19/jcli-d-18-0700.1.xml, publisher: American Meteorological Society Section: Journal of Climate

Yong Z, Xiong J, Wang Z, et al (2021) Relationship of extreme precipitation, surface air temperature, and dew point temperature across the Tibetan Plateau. Climatic Change 165(1-2):41. https://doi.

org/10.1007/s10584-021-03076-2, URL https://link.springer.com/10.1007/s10584-021-03076-2

Zhang W, Villarini G, Wehner M (2019) Contrasting the responses of extreme precipitation to changes in surface air and dew point temperatures. Climatic Change 154(1-2):257–271. https://doi.org/10.1007/s10584-019-02415-8, URL http://link.springer.com/10.1007/s10584-019-02415-8

Zhang X, Zwiers FW, Li G, et al (2017) Complexity in estimating past and future extreme short-duration rainfall. Nature Geoscience 10(4):255–259. https://doi.org/10.1038/ngeo2911, URL http://www.nature.com/articles/ngeo2911